Journal of The Electrochemical Society, **154** (6) B514-B522 (2007)
0013-4651/2007/154(6)/B514/9/$20.00 © The Electrochemical Society

Mixed Potential in a Direct Methanol Fuel Cell

Modeling and Experiments

Fuqiang Liu[a,*,c] and Chao-Yang Wang[a,b,,z]**

[a]*Department of Materials Science and Engineering, and* [b]*Department of Mechanical Engineering, Electrochemical Engine Center, The Pennsylvania State University, University Park, Pennsylvania 16802, USA*

A mathematical model for the cathode of a direct methanol fuel cell (DMFC) is developed to investigate two-phase transport in the catalyst layer (CL) and to elucidate the mechanism of cathode mixed potential due to oxidation of crossover methanol. A coupled model of two-phase species transport and multistep electrochemical kinetics, including simultaneous oxygen reduction, methanol oxidation, and gas phase chemical reaction, is presented. The model predictions agree favorably with experiments of cathode mixed potential, and the predicted profiles of water saturation, oxygen concentration, and overpotential along the CL thickness further reveal the profound interplay between multiple reactions and the transport of oxygen and water. It is shown that in the presence of methanol crossover, the DMFC cathode is operated at higher overpotential and water saturation, with larger oxygen transport loss than that in the H_2/air counterpart. The model results also indicate that reducing the cathode CL thickness can facilitate both liquid water removal and oxygen transport through the CL, leading to improved cathode performance.
 [DOI: 10.1149/1.2718404]

Manuscript submitted September 27, 2006; revised manuscript received January 22, 2007. Available electronically April 4, 2007.

A primary factor limiting direct methanol fuel cell (DMFC) performance is methanol crossover through the electrolyte membrane.[1-3] This includes loss of methanol fuel from the anode and performance loss at the cathode, where simultaneous reduction of O_2 (ORR) and oxidation of methanol (MOR) lead to lower cathode potential and hence, decreased cell voltage.[3]

Cathode mixed potential has been the subject of numerous experimental studies. Bittinscattaneo et al.[4] investigated the interaction of methanol and oxygen at a poly(tetrafluoroethylene) (PTFE)-bonded gas diffusion electrode and found that MOR partial current was enhanced and the onset of MOR occurred 100 mV more cathodic in the presence of oxygen. Chu and Gilman[5] claimed, however, that the ORR rate was reduced by surface poisoning of methanol oxidation fragments or organic impurities in the methanol. Similar results were reported by Paulus et al.,[6] but the ORR was proven to be unaffected by the presence of methanol. Vielstich et al.[7] proposed a purely chemical reaction between oxygen and methanol at the platinum interface in a gas diffusion electrode. It was found that this chemical pathway, accompanied by a strong increase in the fuel consumption rate, considerably decreases the ORR. Recently, Jusys and Behm[8] determined separately the rates of the simultaneous MOR and ORR on Pt/C in O_2-saturated methanol solution. Their results showed a slight deviation of the net current from the simple additive superposition of ORR and MOR currents, due to an increased formation of partly oxidized by-products. The conclusions from different groups are controversial; therefore, in spite of extensive studies, a full mechanistic understanding of the mixed potential in the DMFC cathode remains elusive.

Several numerical models have been developed to describe DMFC behaviors due to strong interest in DMFC technology for portable and micropower. Wang and Wang[9] presented a multicomponent model for a liquid-feed DMFC. The two-phase transport in porous backing layers was elaborated in the model, the catalyst layer (CL) was treated as an interface, and the effective cathodic current density was treated as a summation of the load current and methanol crossover current to account for the crossover effect.[9] Murgia et al.[10] and Raman et al.[11] proposed a one-dimensional, multicomponent model and studied the effects of cathode flooding and methanol crossover overpotential with different oxidants. Most recently, Kulikovsky[12,13] has developed a one-dimensional (1D) + 1D model of a DMFC based on semiempirical equations. This model predicts formation of a narrow zone of local current, which short-circuits cell electrodes even at small current. While the above-mentioned studies touched upon some fundamental issues of species transport and electrochemical reaction in a DMFC, the most important ORR and MOR kinetics and their mutual interactions have not been addressed in sufficient detail. To our best knowledge, there is no reliable model to accurately estimate the crossover effect on cathode performance in a DMFC.

The objective of the present study is twofold. The first goal is to introduce a 1D model of the DMFC cathode incorporating recent experimental findings on electrochemical kinetics as well as the multiphase mixture (M^2) model of two-phase transport developed by Wang et al.[14-19] Considering the highly flooded nature of a DMFC cathode, the two-phase description is essential. The combination of these two aspects, therefore, permits a more accurate modeling of the mixed potential due to methanol crossover, as well as its interactions with the transport of gaseous oxygen and liquid water across the CL. The second objective is to optimize CL thickness. Model predictions of cathode CL performance for various thicknesses are given, and the full effects of two-phase transport and multistep electrochemical kinetics are discussed.

Model

The M^2 model for two-phase transport is combined with a multistep kinetic model in this work. General assumptions made in this study are that (*i*) the system is assumed to be isothermal and at steady state, (*ii*) at the reaction interface, O_2 diffusion resistance through the ionomer film is negligible due to the small film thickness (i.e., ~5 nm), and (*iii*) the proton conductivity of the membrane is taken as a constant due to sufficient hydration in the DMFC environment.

Two-phase transport model.— The M^2 formulation is used to describe two-phase species transport in the DMFC cathode. Readers are referred to references[14-19] for details of this model. Here, only a brief description is given. Figure 1 shows a schematic of the 1D computational domain and related transport processes. The governing equations consist of those for the conservation of oxygen, methanol, water, and proton species and charge conservation, along with appropriate sink/source terms, as summarized in Table I. Some of the equations are taken from Pasaogullari and Wang[16] and modified for use in a DMFC system of interest in this work. Several key features of the present model are noteworthy as discussed below.

The governing equation to describe water transport in the CL can be expressed as

* Electrochemical Society Student Member.
** Electrochemical Society Active Member.
[c] Present address: United Technologies Research Center, East Hartford, Connecticut 06108, USA.
[z] E-mail: cxw31@psu.edu

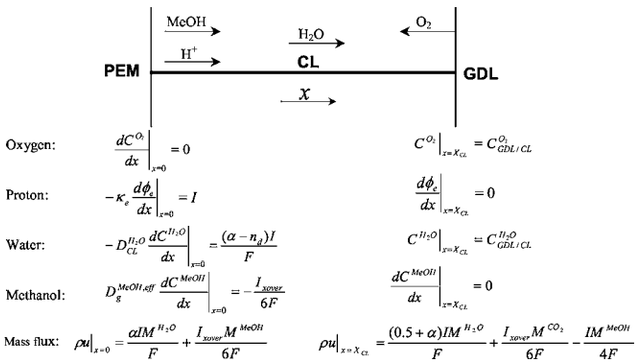

Figure 1. Schematic representation of one-dimensional computational domain and related transport processes in the cathode CL. Boundary conditions at two interfaces are also given.

$$\frac{d}{dx}(\gamma_c u C^{\mathrm{H_2O}}) + \frac{d}{dx}\left[\left(\frac{1 - C_l^{\mathrm{MeOH}} M^{\mathrm{MeOH}}/\rho}{M^{\mathrm{H_2O}}} - \frac{C_{\mathrm{sat}}^{\mathrm{H_2O}}}{\rho_g}\right) j_l\right] + \frac{d}{dx}\left(\frac{n_d}{F} I_e\right) = S^{\mathrm{H_2O}} \quad [1]$$

The three terms on the left side describe water transport by convection, capillary forces, and electro-osmotic drag, and the right side stands for the source term due to water production. Here, I_e is the ionic current density conducted passing through the electrolyte in the CL, $C_l^{\mathrm{MeOH}} M^{\mathrm{MeOH}}/\rho_l$ the mass fraction of methanol in the liquid, u the superficial two-phase mixture velocity, and γ_c the advection factor expressed as

$$\gamma_c = \begin{cases} \dfrac{\rho}{C^{\mathrm{H_2O}}}\left(\dfrac{\lambda_l}{M^{\mathrm{H_2O}}} + \lambda_g \dfrac{C_{\mathrm{sat}}^{\mathrm{H_2O}}}{\rho_g}\right) & \text{for water} \\ \dfrac{\rho \lambda_g}{\rho_g (1 - s)} & \text{for other species} \end{cases} \quad [2]$$

where ρ, λ_l, and λ_g are the two-phase mixture density, relative mobility of liquid and gas phases, respectively, namely

$$\rho = \rho_l s + \rho_g (1 - s) \quad [3]$$

$$\lambda_l = \frac{k_{rl}/v_l}{k_{rl}/v_l + k_{rg}/v_g} \qquad \lambda_g = 1 - \lambda_l \quad [4]$$

where k_{rg} and k_{rl} are the relative permeabilities of individual phases, which are assumed to be the cubic function of phase saturations.

In Eq. 1, j_l is the liquid flux driven by capillary pressure gradient as given by

$$j_l = \frac{\lambda_l \lambda_g \rho K}{\mu} \frac{d}{dx}\left(\sigma \cos(\theta_C)\left(\frac{\varepsilon}{K}\right)^{1/2} J(s)\right) \quad [5]$$

where $J(s)$ is the Leverett function and is given for both hydrophilic and hydrophobic media as[16]

$$J(s) = \begin{cases} 1.417(1 - s) - 2.120(1 - s)^2 + 1.263(1 - s)^3, & \text{if } \theta_c < 90^\circ \\ 1.417 s - 2.120 s^2 + 1.263 s^3, & \text{if } \theta_c > 90^\circ \end{cases} \quad [6]$$

where θ_c is the contact angle.

The total molar concentration of water in the two-phase mixture is defined as

$$C^{\mathrm{H_2O}} = \frac{\rho_l s}{M^{\mathrm{H_2O}}} + (1 - s) C_{\mathrm{sat}}^{\mathrm{H_2O}} \quad [7]$$

Thus

$$\frac{dC^{\mathrm{H_2O}}}{dx} = \left(\frac{\rho_l}{M^{\mathrm{H_2O}}} - C_{\mathrm{sat}}^{\mathrm{H_2O}}\right)\frac{ds}{dx} \quad [8]$$

Substituting Eq. 2, 5, and 8 into Eq. 1 yields the governing equation for water transport as shown in Table I, where $D_{\mathrm{CL}}^{\mathrm{H_2O}}$ is expressed as

$$D_{\mathrm{CL}}^{\mathrm{H_2O}} = -\frac{\dfrac{1 - C_l^{\mathrm{MeOH}} M^{\mathrm{MeOH}}/\rho}{M^{\mathrm{H_2O}}} - \dfrac{C_{\mathrm{sat}}^{\mathrm{H_2O}}}{\rho_g}}{\dfrac{\rho_l}{M^{\mathrm{H_2O}}} - C_{\mathrm{sat}}^{\mathrm{H_2O}}} \frac{\lambda_l \lambda_g \rho}{\mu} \sigma \cos(\theta_C)(\varepsilon K)^{1/2} \frac{dJ(s)}{ds} \quad [9]$$

In the governing equations for both oxygen and methanol as listed in Table I, diffusion in liquid is neglected due to low O_2 solubility and liquid methanol diffusivity. The effective diffusivities of oxygen and methanol in the gas phase are described by the percolation theory[20-22] as

$$D_{\mathrm{CL}}^{i,\mathrm{eff}} = D_g^i \left(\frac{\varepsilon_{\mathrm{CL}}(1 - s) - X_0}{1 - X_0}\right)^2 \quad [10]$$

where D_g^i, $\varepsilon_{\mathrm{CL}}$, and X_0 are the bulk species diffusivity, porosity of the CL, and percolation critical value, respectively. Values of these parameters can be found in Table II.

Due to thermodynamic equilibrium between the gas and liquid phases, Henry's law is employed to calculate the methanol vapor pressure[9]

$$p_g^{\mathrm{MeOH}} = k_H x_l^{\mathrm{MeOH}} \quad [11]$$

where k_{H} and x_l^{MeOH} are the Henry constant and methanol molar fraction in the liquid, respectively. For dilute solutions the molar concentration of methanol vapor can thus be simply determined by

Table I. Governing equations for the DMFC cathode catalyst layer.

	Conservation equation	Source term
Proton	$\frac{d}{dx}\left(\kappa_e \frac{d\phi_e}{dx}\right) + S^{\Phi} = 0$	$S^{\Phi} = -j_{rxn}^{\mathrm{O_2}} + j_{oxi}^{\mathrm{MeOH}}$
Water	$\frac{d}{dx}(\gamma_c u C^{\mathrm{H_2O}}) = \frac{d}{dx}\left(D_{\mathrm{CL}}^{\mathrm{H_2O}} \frac{dC^{\mathrm{H_2O}}}{dx}\right) - \frac{d}{dx}\left(\frac{n_d}{F} I_e\right) + S^{\mathrm{H_2O}}$	$S^{\mathrm{H_2O}} = \frac{j_{rlx}^{\mathrm{O_2}}}{2F} - \frac{j_{oxi}^{\mathrm{MeOH}}}{6F} + 2r$
Oxygen	$\frac{d}{dx}(\gamma_c u C^{\mathrm{O_2}}) = \frac{d}{dx}\left(D_{g,\mathrm{CL}}^{\mathrm{O_2,eff}} \frac{dC^{\mathrm{O_2}}}{dx}\right) + \frac{d}{dx}\left(\frac{C^{\mathrm{O_2}}}{\rho_g} j_l\right) + S^{\mathrm{O_2}}$	$S^{\mathrm{O_2}} = -\frac{j_{rxn}^{\mathrm{O_2}}}{4F} - 1.5r$
Methanol	$\frac{d}{dx}(\gamma_c u C^{\mathrm{MeOH}}) = \frac{d}{dx}\left(D_g^{\mathrm{MeOH,eff}} \frac{dC_g^{\mathrm{MeOH}}}{dx}\right) - \frac{d}{dx}\left[\left(\frac{C_l^{\mathrm{MeOH}}}{\rho_l} - \frac{C_g^{\mathrm{MeOH}}}{\rho_g}\right) j_l\right] + S^{\mathrm{MeOH}}$	$S^{\mathrm{MeOH}} = -\frac{j_{oxi}^{\mathrm{MeOH}}}{6F} - r$

Where r is the gas-phase chemical reaction rate between methanol vapor and oxygen.

Table II. Parameters used in calculations.

Parameters	Value
Anode limiting current density, $I_{A,\text{lim}}$ (mA/cm^2)	290
Air pressure in gas channel inlet, p (kPa)	100
Cathode gas viscosity, ν_g (m^2/s)	2.06×10^{-5}
CL permeability at reference porosity (0.25), K^0_{CL} (m^2)	2.0×10^{-15}
Concentration exponent of methanol, β	1.9
Concentration exponent of oxygen, γ	0.01
Contact angle of CL, θ_{CL} (°)	10
Contact angle of GDL, θ_{GDL} (°)	120
GDL permeability, K_{GDL} (m^2)	5.0×10^{-13}
Henry's law constant, k_H (Pa)	145696
Intrinsic proton conductivity of fully hydrated polymer, $\kappa_{e,0}$ (S/cm)	0.1
Liquid-water viscosity, ν_l (m^2/s)	3.49×10^{-7}
Methanol vapor diffusion coefficient, D_g^{MeOH} (m^2/s)	1.89×10^{-5}
Net water transport coefficient, α	0.8
Operating temperature, T (°C)	60
Oxygen diffusion coefficient, $D_g^{\text{O}_2}$ (m^2/s)	1.29×10^{-5}
Percolation critical value, X_0	0.085
Porosity of the GDL, ε_{GDL}	0.4
Proportionality constant of MOR, K	1.0×10^7
Reactive area per volume, a (m^2/m^3)	400
Reference exchange current density of ORR, i_0 (A/m^2)	1.5×10^{-5}
Reference oxygen concentration, $c_{\text{O}_2,\text{ref}}$ (mol/m^3)	4.12
Reference porosity of CL, $\varepsilon^0_{\text{CL}}$	0.25
Saturated water vapor molar concentration, $C_{\text{sat}}^{\text{H}_2\text{O}}$ (mol/m^3)	7.20
Surface tension, σ (N/m)	0.0625
Thermodynamic equilibrium potential of ORR (60°C and 1 atm), U_o (V)	1.19
Thickness of the GDL, ΔX_{GDL} (μm)	300
Transfer coefficient of cathode, α_c	1.0

$$C_g^{\text{MeOH}} = \frac{p_g^{\text{MeOH}}}{RT} = \frac{k_{\text{H}}}{RT}\frac{M^{\text{H}_2\text{O}}}{\rho_l^{\text{H}_2\text{O}}}C_l^{\text{MeOH}} \quad [12]$$

Electrochemical kinetics.— In a DMFC cathode, reduction of oxygen and oxidation of crossover methanol occur simultaneously. The rate of ORR is governed by the Tafel kinetics as follows

$$j_{rxn}^{\text{O}_2} = -\, i_0^{\text{O}_2} a \frac{(1-s)C^{\text{O}_2}}{C_{0,\text{ref}}^{\text{O}_2}} \exp\left(-\frac{\alpha_c F}{RT}\eta\right) \quad [13]$$

where a is the specific reaction area equal to the total electrochemical active area (ECA) divided by the CL thickness, the term (1-s) describes the fraction of ECA that is available for ORR in the presence of liquid water, $C_{0,\text{ref}}^{\text{O}_2}$ is the reference oxygen concentration, and α_c is the cathodic transfer coefficient. The cathode overpotential, η, is defined as

$$\eta = V_c - \phi_e - U_o \quad [14]$$

where U_o is the thermodynamic potential of a particular reaction.

In the present model the MOR is considered a multistep reaction and its kinetics is based on the following reaction mechanism[23,24]

$$\text{CH}_3\text{OH} \underset{k_1'}{\overset{k_1}{\leftrightarrow}} \text{CH}_3\text{OH}_{\text{ads}} \quad [15]$$

$$\text{CH}_3\text{OH}_{\text{ads}} \xrightarrow{k_2} \text{CO}_{\text{ads}} + 4\text{H}_{\text{ads}} \quad [16]$$

$$\text{H}_2\text{O} \underset{k_3'}{\overset{k_3}{\leftrightarrow}} \text{OH}_{\text{ads}} + \text{H}_{\text{ads}} \quad [17]$$

$$\text{CO}_{\text{ads}} + \text{OH}_{\text{ads}} \xrightarrow{k_4} \text{CO}_2 + \text{H}_{\text{ads}} \quad [18]$$

$$\text{H}_{\text{ads}} \xrightarrow{k_5} \text{H}^+ + \text{e}^- \quad [19]$$

Here H_{ads} produced in Eq. 16, 17, and 18 is immediately oxidized via Eq. 19 when the potential is above 0.3 V,[23] so the surface coverage of H_{ads} is assumed to be zero at the cathode. At steady state, the surface coverage of different species is constant with time. Following the procedure described by Nordlund and Lindbergh,[24] one can obtain the following species surface coverage

$$\theta_{\text{CO}} = b\frac{k_2 \exp\left(\frac{\alpha_2 F V_{\text{cath}}}{RT}\right)}{k_4 \exp\left(\frac{(1-\beta_4)F V_{\text{cath}}}{RT}\right)} \quad [20]$$

Table III. MOR kinetic parameters.

Parameters	Value
Gas-phase chemical reaction constant, K_r	4.5×10^{-3}
k^1 (m/s)	4.0×10^{-12}
k_1' mol/(m^2 s)	1.54×10^{-10}
k_2 mol/(m^2 s)	3.6×10^{-16}
k_3 mol/(m^2 s)	1.2×10^{-13}
k_3' mol/(m^2 s)	1.3
k_4 mol/(m^2 s)	2.0×10^{-2}
α_2	0.80
β_3	0.5
β_4	0.5

$$\theta_{OH} = \frac{k_1 C^{MeOH}(1 - \theta_{CO})}{b\left[k_1' + k_2 \exp\left(\frac{\alpha_2 F V_{cath}}{RT}\right) + k_1 C^{MeOH}\right] + k_1 C^{MeOH}} \quad [21]$$

where k_i, α_i, and β_i are rate constants, transfer coefficients, and symmetry factors of respective reactions, which are listed in Table III. In the above equations, V_{cath} varies along the thickness of CL, and so does MOR kinetics. Note that here we extend the MOR models of Kauranen and Skou,[23] and Nordlund and Lindbergh[24] on PtRu catalysts to the Pt surface of the DMFC cathode. Thus, some of the kinetic parameters are directly taken from Ref. 24, while others are modified to include special features of MOR on Pt electrodes, e.g., positive shift of peak potential and higher oxidation onset voltage.

In the above two equations, b is expressed as

$$b = \frac{k_3' \exp\left(-\frac{\beta_3 F V_{cath}}{RT}\right)}{\left[k_1' + k_2 \exp\left(\frac{\alpha_2 F V_{cath}}{RT}\right)\right] k_3 \exp\left(\frac{(1-\beta_3) F V_{cath}}{RT}\right)/(k_1 C^{MeOH}) + k_2 \exp\left(\frac{\alpha_2 F V_{cath}}{RT}\right)} \quad [22]$$

where C^{MeOH} represents the molar concentration of methanol in the two-phase mixture, i.e.

$$C^{MeOH} = s C_l^{MeOH} + (1 - s) C_g^{MeOH} \quad [23]$$

The rate-determining step was proposed to be the electrochemical reaction between adsorbed CO and OH. Thus, the MOR current is proportional to the rate of Reaction 18, described as

$$j_{oxi}^{MeOH} = 6aFKk_4 \exp\left(\frac{(1-\beta_4) F V_{cath}}{RT}\right) \theta_{CO} \theta_{OH} \quad [24]$$

where K is a proportionality constant. The concentration dependence of the MOR polarization is shown in Fig. 2, where the pure kinetics is plotted, omitting any mass-transfer limitation. It is seen from Fig. 2 that there is negligibly small current density until the electrode potential is beyond 0.4 V. The MOR current density then increases with the electrode potential until reaching a peak, after which the current density decreases due to surface hydroxide formation, blocking further reaction.[25]

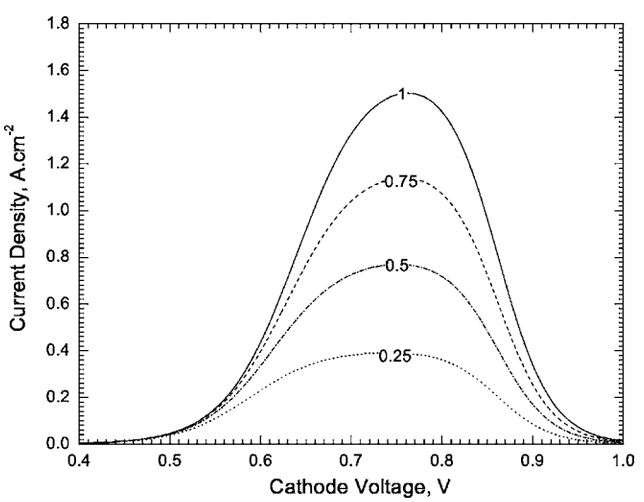

Figure 2. Predicted methanol oxidation current density in the cathode by the present model. The temperature is 60°C and concentrations of methanol are 0.25, 0.5, 0.75, and 1.0 M.

In addition, a purely chemical gas-phase reaction between methanol vapor and oxygen at the Pt surface[7] in the cathode is considered in the present model

$$CH_3OH + 1.5O_2 \rightarrow 2H_2O + CO_2 \quad [25]$$

The chemical reaction rate can be described as

$$r = aK_r (C_g^{MeOH})^{\beta} (C^{O_2})^{\gamma} \quad [26]$$

where K_r is a rate constant, and β and γ are concentration exponents. This chemical reaction consumes additional oxygen and yields a severe concentration gradient across the cathode CL.

In the present model for the DMFC cathode, the mutual interaction between ORR and MOR is reflected in the source term for the equation governing proton transport. As discussed earlier, there are two contradicting opinions in the literature: (*i*) the ORR activity decreases while MOR rate remains constant, or (*ii*) the MOR rate decreases while ORR remains unaltered. For simplicity, additive superposition of the two partial processes is adopted in this work, because each of the two simultaneous reactions is only slightly affected by the other.[8,23] Therefore, the source term in the proton-transport equation is a simple summation of the MOR and ORR currents. The cathode potential, where the MOR and ORR produce zero net current, is referred to as the mixed potential at open circuit. Finally, note that both electrochemical and chemical reactions contribute to the source terms for the transport of oxygen, methanol, and water, as shown in Table I.

Boundary conditions.— The boundary conditions for the conservation equations are listed in Fig. 1. At the interface between the proton exchange membrane (PEM) and cathode CL, the flux conditions for protons, water, methanol, and oxygen as listed in Fig. 1 are self-explanatory, with the total mass flux consisting of methanol and water crossing over the PEM.

At the CL/GDL interface, the water concentration can be prescribed as

$$C_{GDL/CL}^{H_2O} = \frac{\rho_l s_{GDL/CL}}{M^{H_2O}} + (1 - s_{GDL/CL}) C_{sat}^{H_2O} \quad [27]$$

with the liquid saturation at the CL/GDL interface obtained following Pasaogullari and Wang.[15] Similarly, the oxygen concentration at the CL/GDL interface can be calculated from the value in the gas channel, $C_{chann}^{O_2}$, which is obtained by averaging the inlet and outlet oxygen molar fractions, i.e.

$$C_{chann}^{O_2} = \left(\frac{x_O^{chann} + 0.21}{2}\right) \frac{P}{RT} \quad [28]$$

The oxygen molar fraction at the outlet is given by

$$x_O^{chann} = \frac{0.15 S_R - I - I_{xover}}{0.15 S_R - I - I_{xover}/3 + 0.15 S_R \times \frac{0.79}{0.21}} \frac{P - P_{sat}^{H_2O}}{P} \quad [29]$$

where I_{xover} and S_R are the methanol crossover current density and air stoichiometric ratio at 0.15 A/cm^2, a reference operating current

density chosen in this study. In Eq. 29, $I_{xover}/3$ accounts for the rate of carbon dioxide produced by methanol oxidation. As an important input to the present cathode model, the methanol crossover current physically depends on the anode methanol concentration and membrane transport properties, among others. In the present model for the DMFC cathode only, the methanol crossover current is approximated by a simple relation between the crossover current at open circuit, $I_{xover,oc}$, and anode mass-transport-limiting current, $I_{A,lim}$,[19] i.e.

$$I_{xover} = I_{xover,oc}\left(1 - \frac{I}{I_{A,lim}}\right) \quad [30]$$

The methanol crossover current density at open circuit is taken to be 240 mA/cm^2, as measured in corresponding validation experiments.

Experimental

To obtain experimental data of cathode mixed potential, a 12 cm^2 MEA in the form of a catalyst-coated membrane (CCM) based on a Nafion 112 membrane is utilized. The catalyst loadings are 4.5 mg PtRu/cm^2 and 1.2 mg Pt/cm^2 at the anode and cathode, respectively. The cell is operated at 60°C and ambient pressure on both sides. More details of the MEA fabrication, cell fixture, and operating conditions have been detailed elsewhere.[26-28] Under DMFC operation, the anode and cathode stoichiometries of 2.0 and 3.0 at 150 mA/cm^2 are used, representing practically reasonable flow rates for portable applications. To quantify the effect of cathode mixed potential due to the presence of methanol crossover, the H_2/air cell performance is also recorded at the same air flow rate, but the anode H_2 stoichiometry is equal to 8.3 at 150 mA/cm^2, sufficiently large to avoid any appreciable influence from the H_2 anode. Each voltage data point is obtained by averaging the values recorded for 3–5 min at a certain current density. High-frequency resistance (HFR) of the cell at each current density is measured using an Agilent 4338B milliohmmeter at 1 kHz.

DMFC cathode performance is evaluated according to the procedure described by Thomas et al.,[29] i.e.

$$E_{Air}^{MeOH}(I) = E_{MeOH/Air}(I) + E_{MeOH/H_2}(I) \quad [31]$$

where $E_{Air}^{MeOH}(I)$ is the air cathode potential under DMFC conditions that contains the effects of methanol crossover and mixed potential, and $E_{MeOH/Air}(I)$ and $E_{MeOH/H_2}(I)$ are the iR-free voltages measured under DMFC and anode polarization modes.

Results and Discussion

Figure 3 compares the simulated and measured cathode performance in a DMFC and an H_2/air cell at 60°C with the air stoichiometry of 3 at 150 mA/cm^2. Note that V_{cath} at PEM/CL interface was taken as the iR-corrected cathode performance, by assuming that the membrane phase potential is zero at the interface. The steady-state DMFC and anode polarization data are also displayed in the figure for reference. Cathode data points in the DMFC case with current density higher than 250 mA/cm^2 could not be obtained because of the limited methanol transport at the anode. Note that summing the experimental iR-free voltages measured under DMFC and anode polarization modes, followed by correction by DMFC cell resistance, gives the black triangle data points in Fig. 3. It can be seen that the model has excellent agreement with experimental data. Methanol crossover and its detrimental effect diminish with the operating current density, and vanish when the current density is higher than the anode limiting current (i.e., 290 mA/cm^2) where the cathode potential in a DMFC consequently approaches that in the H_2/air cell. This finding is slightly different from the data reported in the literature, where DMFC cathodes still suffer from methanol crossover at very high current densities, or even through entire polarization curves. This is because a very high methanol flow rate (real stoichiometry >10) is commonly employed; therefore it is not surprising to observe high methanol crossover and its detrimental effect at high current densities. Finally, it is interesting to note from Fig. 3 that the cathode voltage loss due to methanol crossover is predicted to be ~40 mV at 150 mA/cm^2, a common current density designed for portable applications.

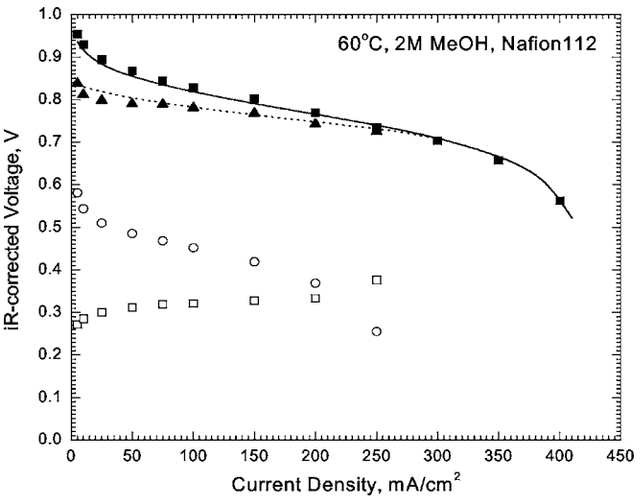

Figure 3. Experimental-model comparison of cathode polarization: (■) iR-corrected H_2/air experimental data, and (▲) iR-corrected DMFC experimental data. The solid and dotted lines are simulated results for the cathode with and without methanol crossover. Other data provided as reference are (□) iR-corrected DMFC anode polarization and (○) iR-corrected DMFC cell performance.

Driven by molecular diffusion and electro-osmotic drag,[30] methanol permeates through the polymer membrane and eventually reacts electrochemically or chemically with oxygen at the cathode platinum surface. The ratio of methanol from chemical oxidation with oxygen to the overall oxidation rate, evaluated from the various source terms of methanol in Table I, ranges from 31% at 5 mA/cm^2 to 8.3% at 100 mA/cm^2. This indicates that electrochemical oxidation consumes most of the crossover methanol, resulting in a mixed cathode potential. To fully understand the mixed potential of an air cathode in the presence of methanol crossover, polarization curves under different cathode environments predicted by the present model are compared, including (*i*) air with methanol crossover, (*ii*) air with methanol crossover and infinite oxygen diffusivity, (*iii*) air without methanol crossover, (*iv*) oxygen with methanol crossover, and (*v*) oxygen without methanol crossover. The results are summarized in Fig. 4. Curves (3) and (5) show the cathode performance using air and oxygen without methanol crossover, respectively. When oxygen is used, the cathode performance improves by ~80 mV in both kinetic and ohmic regimes. In the presence of methanol crossover at the cathode, the performance using air and oxygen is displayed by curves (1) and (4). The open-circuit voltage (OCV) loss due to methanol crossover is almost 100 mV using air, compared to only 20 mV with oxygen; and at 50 mA/cm^2, the cathode voltage is lowered due to methanol crossover by ~66 and 21 mV for air and oxygen, respectively. Therefore, the detrimental effect of methanol crossover is more pronounced when air is used at the oxidant. These simulated results are consistent with our experimental observations (not shown) and the reported crossover overpotential for air and oxygen.[11] The reason is that higher concentration of pure oxygen positively shifts the cathode potential, leading to a higher OH coverage on Pt catalysts and thus a reduction in the parasitic current of MOR. The present explanation can further be verified by curve (2) in Fig. 4, in which oxygen diffusivity in air was set at infinity. The DMFC cathode performance improves dramatically at high current densities, but only slightly at small current densities. This indicates that at small load the improved oxygen diffusion in curve (2) does not contribute as much as the oxygen enrichment, thus leading to the same mixed potential as in curve (1).

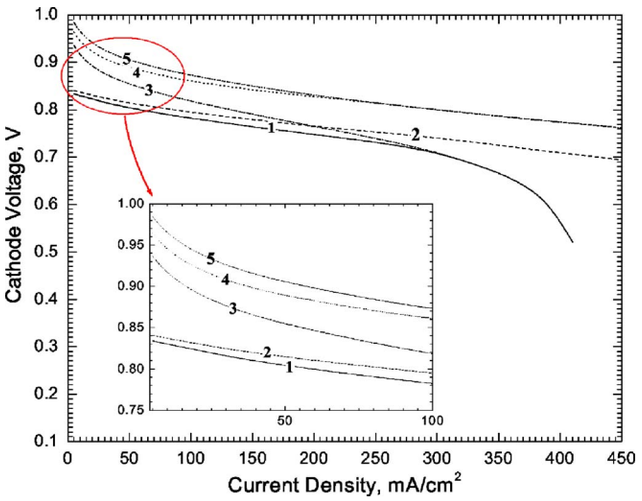

Figure 4. (Color online) Cathode polarization curves under (1) air with MeOH crossover, (2) air with MeOH crossover and infinite oxygen diffusivity, (3) air without MeOH crossover, (4) oxygen with MeOH crossover, and (5) oxygen without MeOH crossover.

The crossover methanol from the anode is almost completely converted to carbon dioxide and water[31] in the presence of cathode catalysts; however, this reaction consumes oxygen from the air supplied to the cathode that would otherwise be needed for the ORR.[32] Figures 5-7 compare oxygen concentration, overpotential, and water saturation profiles in a DMFC cathode (with methanol crossover) with an H_2/air cathode (without methanol crossover). From Fig. 5a, it is clear that the oxygen concentration decreases dramatically from the CL/GDL interface toward the inside of the DMFC cathode, indicating that oxygen is relatively deficient in the CL when methanol crossover is high. For the CL without methanol crossover, however, there is a negligible oxygen concentration gradient across the cathode CL. At high current densities, oxygen concentration profiles in the CL with and without methanol crossover converge to each other where methanol crossover becomes negligible. Water saturation and overpotential profiles in the CL exhibit a similar trend, as shown in Fig. 6 and 7. Water saturation and overpotential are much higher in the CL with methanol crossover than those without crossover, especially at low current densities. Extra water produced from MOR results in an additional mass-transport resistance. These results clearly demonstrate that DMFC cathodes are easily flooded and exhibit considerable mass-transfer resistance.

The influence of MOR parameters, such as methanol crossover current density and kinetic rate constant K in Eq. 24, is explored in Fig. 8 and 9. As seen, the methanol crossover current density at open circuit primarily influences the OCV and cathode performance at small current densities. A larger methanol crossover leads to a low cell voltage in the current range from open circuit to $\sim$300 mA/cm^2. At high operating current densities where methanol crossover diminishes, the effect of methanol crossover is alleviated and all the curves converge to a single one. The MOR kinetic rate constant K is a parameter to quantify methanol tolerance of the cathode catalyst. In this model, ORR kinetics is assumed to be unaffected by the presence of methanol; therefore, small K means that the catalyst is relatively inert to MOR and highly selective toward ORR. Figure 9 shows that smaller K results in smaller overpotential and hence better performance, and leaves higher methanol concentration in the cathode CL. Note that the methanol crossover current density is identical in all cases; thus, it is clear that crossover methanol is detrimental to cathode performance only if oxidized electrochemically. For higher K, for example, $K = 1.0 \times 10^7$, methanol concentration drops dramatically from about 1.5 mol/m^3 at the PEM/CL interface down to zero at the CL/GDL interface. At the

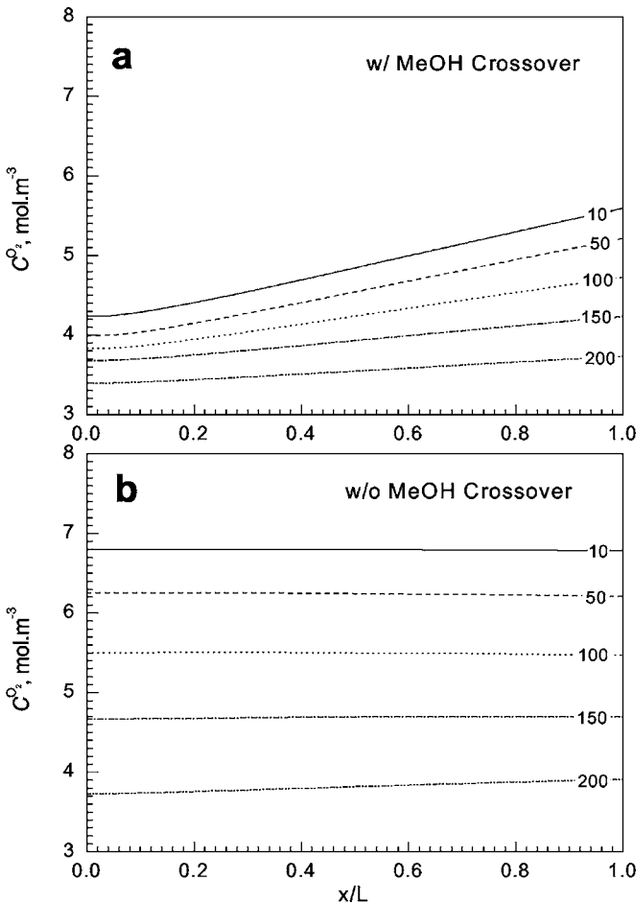

Figure 5. Oxygen concentration profiles along the CL thickness: (a) with MeOH crossover, and (b) without MeOH crossover. Different operating current densities (in mA/cm^2) are indicated in the figures.

same time, the overpotential has to increase to offset the mixed potential and oxygen deficiency in the cathode CL. These results point to essentially two approaches to mitigating the detrimental effect of methanol crossover. One is to block the methanol crossover rate using new polymer materials or MEA design, while the other is to develop and employ methanol-tolerant cathode catalysts, which are required to have higher reactivity toward ORR than MOR.

In a DMFC, high cathode Pt loading is commonly employed to mitigate the methanol crossover effect and enhance the ORR kinetics. However, a higher Pt loading corresponds to a thicker CL, dramatically increasing the resistances of oxygen transport and proton conduction. Reducing CL thickness may be an effective way to improve oxygen transport and hence the cathode performance. Nevertheless, a thinner CL possesses less active reaction sites for ORR, increasing the kinetics loss. Therefore, the thickness of the cathode CL should be optimized to balance the requirements of the electrochemically active area, proton conduction, oxygen diffusion, and water removal under design operating conditions.

Performance of DMFC cathode CLs with various thicknesses is compared in Fig. 10. Thinner CLs show better performance in the mass-transport regime; however, the electrochemical kinetics is impeded by the lower ECA. Thicker CLs show better ORR kinetics at the expense of lower performance in the mass-transport regime at high current densities. Therefore, the optimal CL thickness depends strongly on the operating current density. From the inset of Fig. 10, the 20 μm thick CL displays the highest voltage at 150 mA/cm^2, a design point for portable applications. Optimized performance is attained by good balance between two competing factors: oxygen

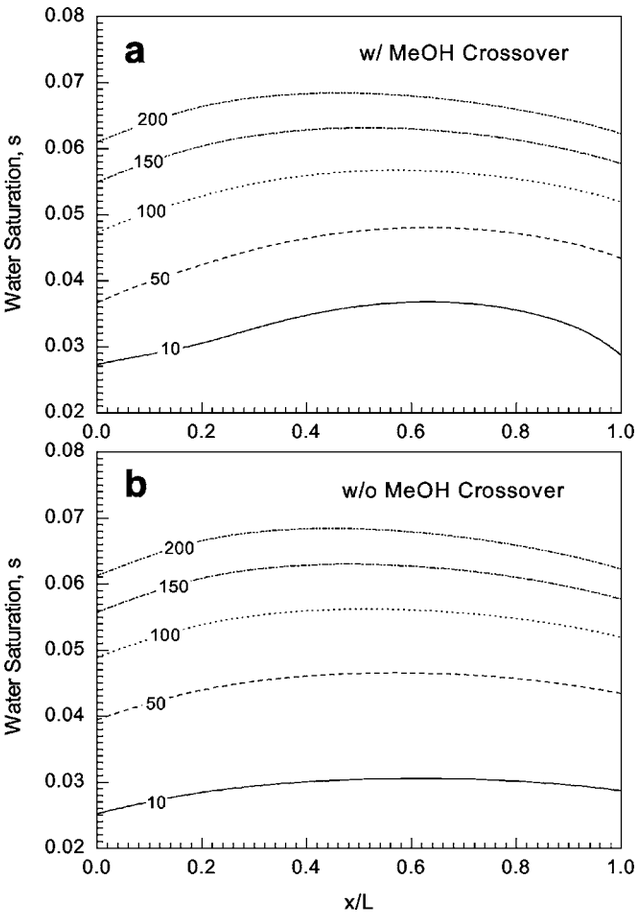

Figure 6. Water saturation profiles along the CL thickness: (a) with MeOH crossover, and (b) without MeOH crossover. Different operating current densities (in mA/cm^2) are indicated in the figures.

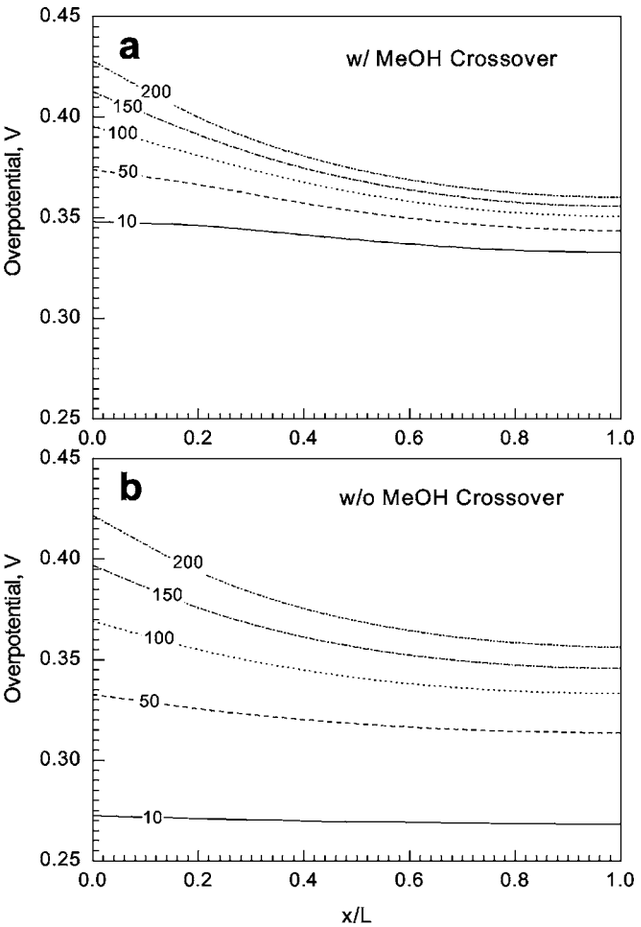

Figure 7. Overpotential profiles along the CL thickness: (a) with MeOH crossover and (b) without MeOH crossover. Different operating current densities (in mA/cm^2) are indicated in the figures.

transport and protonic resistance in the CL, which can be best demonstrated by water saturation and overpotential profiles displayed in Fig. 11 and 12, respectively. Water saturation in thicker cathode CLs is higher because water removal is more difficult; thus, a significant fraction of the catalytic sites is covered by liquid water and cannot contribute to the electrochemical reaction. On the contrary, oxygen transport is more favorable in thinner CLs, leading to higher and more uniform oxygen concentration profiles along the thickness at different current densities (not shown here). In Fig. 12, although the overpotential variation across the 10 μm CL at 150 mA/cm^2 is smaller, its magnitude is relatively larger than those of thicker CLs. The 20 μm CL has the smallest overpotential at the PEM/CL interface, indicative of the best cathode performance, due to the optimal combination of active catalytic sites and mass transport/proton conduction.

Conclusion

A mathematical model has been developed for the DMFC cathode and is validated against experimental data with excellent agreement. The model incorporates the two-phase, multicomponent species transport, multistep electrochemical kinetics, and a chemical pathway between methanol and oxygen vapor, all of which are essential for accurate prediction of species distribution, polarization curve, and mixed potential due to methanol crossover.

The detrimental effect of methanol crossover is found to be more pronounced when air is used at the cathode rather than pure oxygen. The origin of the mixed potential is attributed to deficient oxygen and parasitic MOR current at the DMFC cathode, caused by chemi-

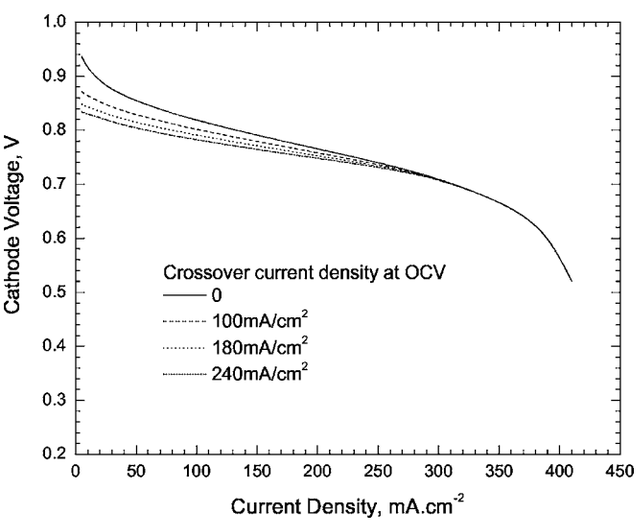

Figure 8. (Color online) Effect of methanol crossover on DMFC cathode performance.

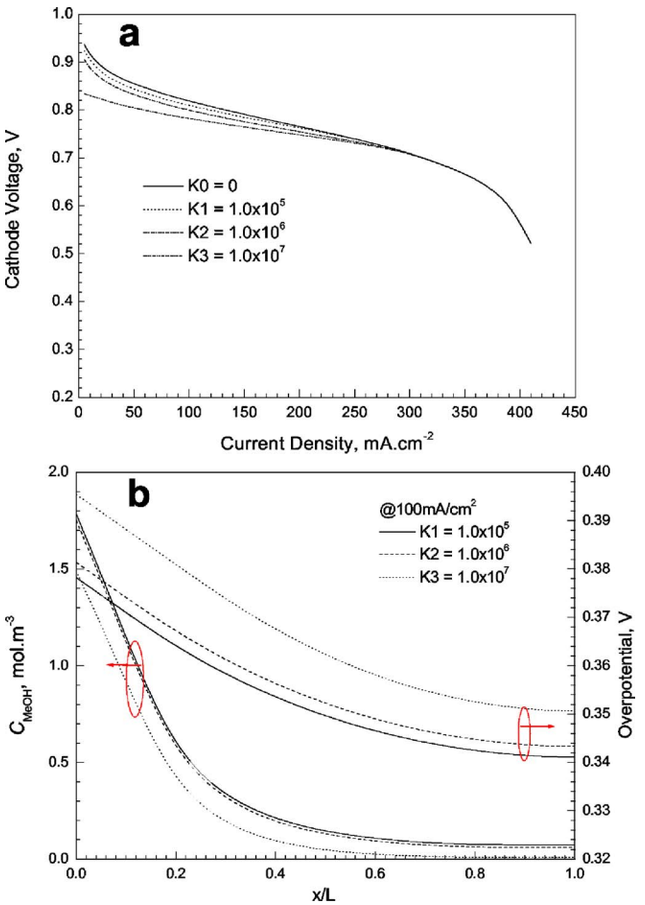

Figure 9. (Color online) Effect of methanol tolerance of the cathode catalyst: (a) on DMFC cathode performance and (b) methanol concentration and overpotential profiles along the CL thickness.

cal and electrochemical oxidation of the crossover methanol. The cathode overpotential therefore has to increase to maintain the prescribed load current. The model predicts that reducing methanol

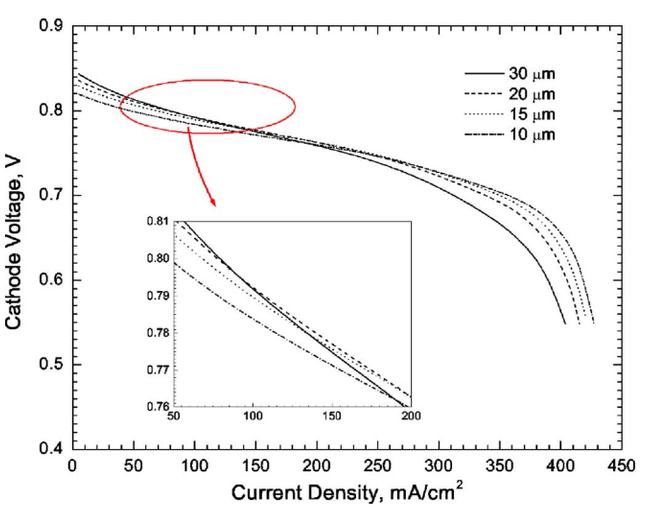

Figure 10. (Color online) DMFC cathode performance with different thickness of CLs. The active surface area (for both ORR and MOR) in each CL is proportional to its thickness.

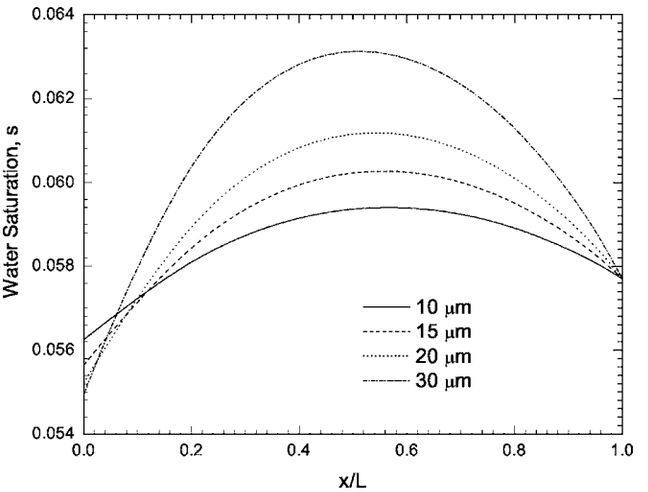

Figure 11. Water saturation profiles along the thickness of cathode CL at 150 mA/cm^2 for different DMFC cathode CLs of varying thickness.

crossover rate and utilizing methanol-tolerant cathode catalysts could be two effective approaches to recover ~40 mV at 150 mA/cm^2 due to methanol crossover. Small methanol crossover corresponds to high OCV as well as high cathode voltage in the kinetics region. Higher reaction selectivity toward the ORR than MOR implies higher methanol tolerance of the cathode catalyst and hence, smaller cathode voltage loss. Optimal cathode CL thickness is found to depend on the operating current density. Oxygen concentration drop across thinner CLs is smaller than that across thicker CLs; however, its overpotential is relatively larger, as a result of fewer catalytic sites. The highest voltage at 150 mA/cm^2 is achieved by a 20 μm CL, representing a trade-off between the electrochemically active area and oxygen/proton transport resistances in the CL.

Acknowledgments

Financial support of this work in part by the DARPA Microsystem Technology Office (MTO) under contract no. DAAH01-1-R001 and ECEC industrial sponsors is gratefully acknowledged.

The Pennsylvania State University assisted in meeting the publication costs of this article.

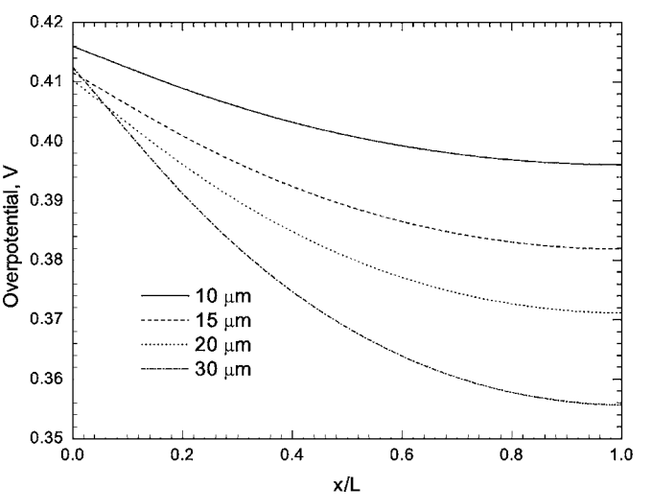

Figure 12. Overpotential profiles along the thickness of cathode CL at 150 mA/cm^2 for different DMFC cathode CLs of varying thickness.

References

1. X. Ren, T. E. Springer, and S. Gottesfeld, *J. Electrochem. Soc.*, **147**, 92 (2000).
2. R. Z. Jiang and D. R. Chu, *J. Electrochem. Soc.*, **151**, A69 (2004).
3. A. S. Arico, S. Srinivasan, and V. Antonucci, *Fuel Cells*, **1**, 133 (2001).
4. B. Bittinscattaneo, S. Wasmus, B. Lopezmishima, and W. Vielstich, *J. Appl. Electrochem.*, **23**, 625 (1993).
5. D. Chu and S. Gilman, *J. Electrochem. Soc.*, **141**, 1770 (1994).
6. U. A. Paulus, T. J. Schmidt, and H. A. Gasteiger, in *Handbook of Fuel Cells-Fundamentals, Technology and Applications*, W. Vielstich, A. Lamm, and H. A. Gasteiger, Editors, Vol. 2, Chap. 38, John Wiley & Sons, Chichester (2003).
7. W. Vielstich, V. A. Paganin, F. H. B. Lima, and E. A. Ticianelli, *J. Electrochem. Soc.*, **148**, A502 (2001).
8. Z. Jusys and R. J. Behm, *Electrochim. Acta*, **49**, 3891 (2004).
9. Z. H. Wang and C. Y. Wang, *J. Electrochem. Soc.*, **150**, A508 (2003).
10. G. Murgia, L. Pisani, A. K. Shukla, and K. Scott, *J. Electrochem. Soc.*, **150**, A1231 (2003).
11. R. K. Raman, G. Murgia, and A. K. Shukla, *J. Appl. Electrochem.*, **34**, 1029 (2004).
12. A. A. Kulikovsky, *Electrochem. Commun.*, **6**, 1259 (2004).
13. A. A. Kulikovsky, *J. Electrochem. Soc.*, **152**, A1121 (2005).
14. U. Pasaogullari and C. Y. Wang, *J. Electrochem. Soc.*, **151**, A399 (2004).
15. U. Pasaogullari and C. Y. Wang, *Electrochim. Acta*, **49**, 4359 (2004).
16. U. Pasaogullari and C. Y. Wang, *J. Electrochem. Soc.*, **152**, A380 (2005).
17. C. Y. Wang and P. Cheng, *Int. J. Heat Mass Transfer*, **39**, 3607 (1996).
18. C. Y. Wang and P. Cheng, *Adv. Heat Transfer*, **30**, 93 (1997).
19. C. Y. Wang, *Chem. Rev. (Washington, D.C.)*, **104**, 4727 (2004).
20. M. Eikerling and A. A. Kornyshev, *J. Electroanal. Chem.*, **453**, 89 (1998).
21. M. Eikerling and A. A. Kornyshev, *J. Electroanal. Chem.*, **475**, 107 (1999).
22. Q. P. Wang, M. Eikerling, D. T. Song, Z. S. Liu, T. Navessin, Z. Xie, and S. Holdcroft, *J. Electrochem. Soc.*, **151**, A950 (2004).
23. P. S. Kauranen and E. Skou, *J. Electroanal. Chem.*, **408**, 189 (1996).
24. J. Nordlund and G. Lindbergh, *J. Electrochem. Soc.*, **149**, A1107 (2002).
25. W. S. Li, L. P. Tian, Q. M. Huang, H. Li, H. Y. Chen, and X. P. Lian, *J. Power Sources*, **104**, 281 (2002).
26. G. Q. Lu, F. Q. Liu, and C. Y. Wang, *Electrochem. Solid-State Lett.*, **8**, A1 (2005).
27. F. Q. Liu, G. Q. Lu, and C. Y. Wang, *J. Electrochem. Soc.*, **153**, A543 (2006).
28. F. Q. Liu and C. Y. Wang, *Electrochim. Acta*, **50**, 1413 (2005).
29. S. C. Thomas, X. Ren, S. Gottesfeld, and P. Zelenay, *Electrochim. Acta*, **47**, 3741 (2002).
30. X. M. Ren, T. E. Springer, T. A. Zawodzinski, and S. Gottesfeld, *J. Electrochem. Soc.*, **147**, 466 (2000).
31. J. T. Wang, S. Wasmus, and R. F. Savinell, *J. Electrochem. Soc.*, **143**, 1233 (1996).
32. J. Müller, G. Frank, K. Colbow, and D. Wilkinson, in *Handbook of Fuel Cells-Fundamentals, Technology and Applications*, W. Vielstich, A. Lamm, and H. A. Gasteiger, Editors, Vol. 4, Chap. 62, John Wiley & Sons, Chichester (2003).